

Generation of Drug-Induced Cardiac Reactions towards Virtual Clinical Trials

Qian Shao^{1*}, Bang Du^{1*}, Zepeng Li¹, Qiyuan Chen¹, Hongxia Xu¹,
Jimeng Sun³, Jian Wu^{1†}, Jintai Chen^{2†}

¹Zhejiang University

²The Hong Kong University of Science and Technology

³University of Illinois Urbana-Champaign
wujian2000@zju.edu.cn, jtchen721@gmail.com

Abstract

Clinical trials remain critical in cardiac drug development but face high failure rates due to efficacy limitations and safety risks, incurring substantial costs. In-silico trial methodologies, particularly generative models simulating drug-induced electrocardiogram (ECG) alterations, offer a potential solution to mitigate these challenges. While existing models show progress in ECG synthesis, their constrained fidelity and inability to characterize individual-specific pharmacological response patterns fundamentally limit clinical translatability. To address these issues, we propose a novel Drug-Aware Diffusion Model (DADM). Specifically, we construct a set of ordinary differential equations to provide external physical knowledge (EPK) of the realistic ECG morphology. The EPK is used to adaptively constrain the morphology of the generated ECGs through a dynamic cross-attention (DCA) mechanism. Furthermore, we propose an extension of ControlNet to incorporate demographic and drug data, simulating individual drug reactions. Compared to the other eight state-of-the-art (SOTA) ECG generative models: 1) Quantitative and expert evaluation demonstrate that DADM generates ECGs with superior fidelity; 2) Comparative results on two real-world databases covering 8 types of drug regimens verify that DADM can more accurately simulate drug-induced changes in ECGs, improving the accuracy by at least 5.79% and recall by 8%. In addition, the ECGs generated by DADM can also enhance model performance in downstream drug-effect classification tasks.

1 Introduction

Cardiac diseases impose a significant burden globally, with drug development in this domain facing disproportionate challenges compared to other therapeutic areas [Fordyce *et al.*, 2015]. A key bottleneck lies in the exorbitant costs of

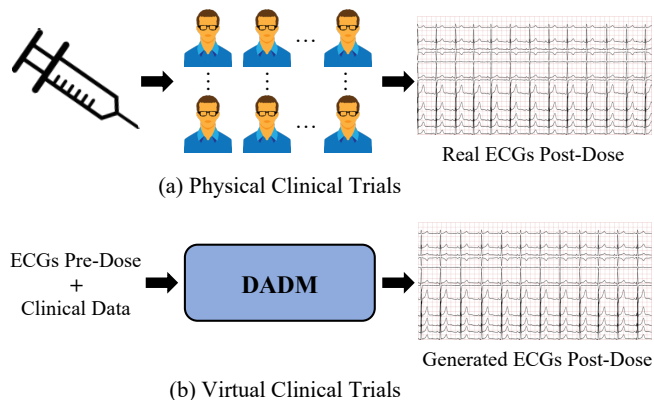


Figure 1: Physical clinical trials v.s. virtual clinical trials. In realistic scenarios, we aim to train the DADM for virtual trials with limited physical trial data, thereby avoiding financial and safety risks associated with large-scale clinical trials.

clinical trials, compounded by high attrition rates across development phases [DiMasi *et al.*, 2016]. Previous analyses show that 79% of failures stem from inadequate efficacy or unforeseen safety issues [Dowden and Munro, 2019], highlighting the critical need for improved predictive tools during early-stage development.

Leveraging generative models to simulate electrocardiogram (ECG) changes induced by drugs is an effective way to conduct virtual clinical trials. As illustrated in Figure 1, this approach harnesses limited physical trial data to train generative models capable of simulating diverse pharmacological responses, thereby mitigating financial risks.

While existing works have demonstrated progress in ECG signal synthesis [Simone and Bacciu, 2023; Chung *et al.*, 2023; Li *et al.*, 2024], two challenges persist when adapting these methods to pharmacodynamic ECG modeling. The first challenge lies in **ensuring that the generated ECGs exhibit realistic PQRST morphology**, a fundamental requirement in ECG generation tasks [Kaplan, 1990; Davey, 1999]. Previous studies have introduced ordinary differential equation (ODE) systems to enhance the authenticity of generated signals, achieving notable advancements. For example, McSharry *et al.* [2003] represents a dynamical model by a system of three ODEs to generate ECGs with realistic PQRST mor-

*These authors contributed equally to this work.

†Corresponding authors.

phology, as well as prescribed heart rate dynamics. Building on this foundation, Golany *et al.* [2020, 2021] design SIMGAN and ECG ODE-GAN, respectively. They leverage ODEs as External Physical Knowledge (EPK) to constrain the generator’s output, ensuring fidelity. However, these methods cannot control the restricting strength of EPK on ECG generation as the time steps iterate, which may undermine the generation quality (see Section 4.7). The second challenge lies in **simulating cardiac drug reactions on ECGs from diverse subjects at various post-dose time points**, an area that remains underexplored.

In this paper, we design a Drug-Aware Diffusion Model (DADM), a novel deep-learning framework capable of generating post-dose ECGs based on pre-dose ECGs and clinical information. To generate realistic ECGs, we first construct a set of ODEs to describe EPK [McSharry *et al.*, 2003]. Then, we propose a dynamic cross-attention (DCA) mechanism for the denoising process, which can adaptively adjust the constraints imposed by the EPK according to the time steps. In the initial generation stage, the model should rely more on EPK to generate basic waveforms. In the later stage, the external control should be reduced to generate more detailed data. To accurately simulate the individual cardiac drug reactions on ECGs, we extend ControlNet [Zhang *et al.*, 2023] to enable it to incorporate both EPK and tabular clinical data, including demographic and drug information, which is named Clinical Information ControlNet (CICN).

We compare DADM with eight other SOTA ECG generative models on two publicly available databases [Johannesen *et al.*, 2014, 2016], comprising a total of 9,443 12-lead ECGs, which cover the effects of 8 drug regimens. The quantitative and expert assessment demonstrates that DADM generates ECGs with superior fidelity. The comparative results verify that DADM can more accurately simulate drug-induced changes in ECGs, improving the accuracy by at least 5.79% and recall by 8%. Furthermore, the ECGs generated by DADM can also enhance model performance in downstream drug-effect classification tasks. And the ablation and visualization results demonstrate the effectiveness of each module.

In summary, the main contributions of this article are as follows:

- We propose the DADM for virtual trials of cardiac drugs by generating drug-induced ECGs.
- We inject the EPK into the denoising steps via the DCA mechanism to ensure that the generated ECGs exhibit realistic PQRST waves.
- We design the CICN to control the model to generate drug-induced ECGs based on demographic information and drug data.
- We validate the superiority of DADM compared with eight SOTA generative models on two public databases, covering the evaluation of the effects of 8 drug regimens.

2 Related Works

Generative methods have been widely used to generate ECGs, *e.g.*, Generative Adversarial Networks (GANs) [Simone and Bacciu, 2023], Autoregressive Models (AMs) [Chung *et al.*,

2023], and Diffusion Models (DMs) [Li *et al.*, 2024]. Researchers design various GANs to generate realistic and personalized ECGs, for example, Golany *et al.* [2020, 2021] integrate physical knowledge into the generation process of GAN to produce realistic ECG signals by using a physically motivated ECG simulator, given by a set of ordinary differential equations [McSharry *et al.*, 2003]. Golany and Radinsky [2019] uses the wave values and durations of ECG signals as constraints for GAN to generate personalized heartbeats. Hu *et al.* [2024] generates digital twins of healthy individuals’ anomalous ECGs and enhances the model sensitivity to the personalized symptoms. Besides GANs, AMs and DMs have also been employed for ECG signal generation, achieving SOTA performance in aiding the diagnosis of cardiac disease. For instance, Chung *et al.* [2023] proposes Auto-TTE, an autoregressive generation model driven by clinical text reports. Neifar *et al.* [2023] introduces a novel versatile approach based on DMs for ECG synthesis. Alcaraz and Strodtz [2023]; Zama and Schwenker [2023] design novel DMs coupled with state space models to generate 12-lead ECGs.

Most of the aforementioned work has primarily focused on aiding cardiac disease diagnosis and has achieved significant progress in this area. In contrast, our work is centered on generating ECGs that reflect drug reactions, thereby enabling virtual clinical trials.

3 Methods

3.1 Overview

In the following sections, we first describe the EPK construction using an ODE system (see Section 3.2). Next, we introduce the workflow of denoising diffusion probabilistic models (see Section 3.3). Then, we describe integrating EPK into the denoising process using the DCA mechanism (see Section 3.4). Finally, we present the design of the CICN (see Section 3.5).

3.2 Ordinary Differential Equation System

We construct an ODE system [McSharry *et al.*, 2003] to describe the EPK, which includes specific heart rate statistics, such as the mean and standard deviation of heart rate, as well as the frequency-domain characteristics of heart rate variability [Malik and Camm, 1990]. The following two sections introduce the specific forms of the ODEs and the numerical solution method, respectively.

Ordinary Differential Equations. The EPK is defined by three coupled ODEs, giving rise to a trajectory $(x(t), y(t), z(t))$. The ODEs are as follows:

$$\begin{aligned}
 \frac{dx}{dt} &= \alpha x - \omega y \equiv f_x(x, y; \eta), \\
 \frac{dy}{dt} &= \alpha y + \omega x \equiv f_y(x, y; \eta), \\
 \frac{dz}{dt} &= - \sum_{i \in \{P, Q, R, S, T\}} a_i \Delta \theta_i \exp\left(-\frac{\Delta \theta_i^2}{2b_i^2}\right) - (z - z_0(t)) \\
 &\equiv f_z(x, y, z, t; \eta),
 \end{aligned} \tag{1}$$

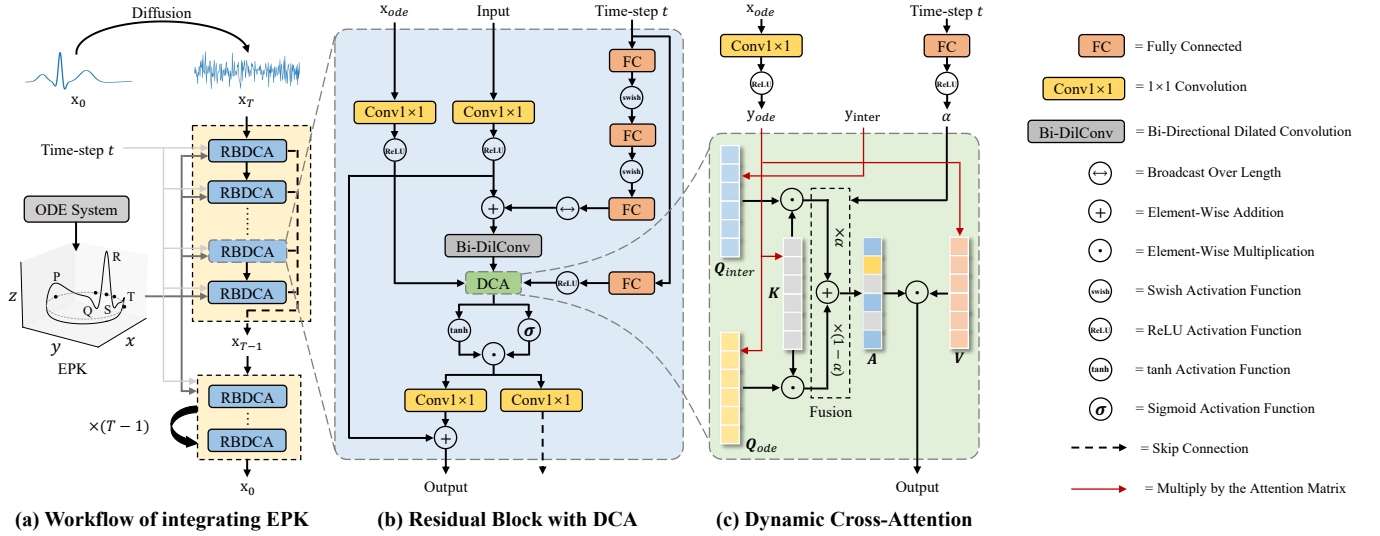


Figure 2: (a) Workflow of integrating EPK; (b) Structure of RBDCA. \mathbf{x}_{ode} represents the external physical knowledge. The output of the previous residual block is the input of the next one. Each block is also connected through a skip connection; (c) Structure of DCA. \mathbf{y}_{inter} and \mathbf{A} represent the output of the Bi-DilConv and the cross-attention map, respectively.

where $\alpha = 1 - \sqrt{x^2 + y^2}$, $\Delta\theta_i = (\theta - \theta_i) \bmod 2\pi$, $\theta = \text{atan2}(y, x)$ (the four quadrant arctangent of the real parts of the elements of x and y , with $-\pi \leq \text{atan2}(y, x) \leq \pi$), and ω is the angular velocity of the trajectory as it moves around the limit cycle. Baseline wander is introduced by coupling the baseline value $z_0(t)$ in (1) to the respiratory frequency f_2 using:

$$z_0(t) = A \sin(2\pi f_2 t),$$

where $A = 0.15\text{mV}$. Baseline wander is a type of low-frequency noise (0.05 – 3Hz during stress testing) [Sörnmo and Laguna, 2005], caused by various factors: respiratory motion, patient movement, poor contact of electrode cables and ECG recording equipment, inadequate skin preparation at the electrode placement sites, and unclear electrodes [Golany *et al.*, 2020]. The solution of equation (1) is a trajectory in three-dimensional space with coordinates $(x(t), y(t), z(t))$. The generated ECG signal is only the third dimension, *i.e.*, $z(t)$, which is the motion trajectory around a unit radius limit cycle on the (x, y) plane. Each complete rotation of this circle corresponds to one heartbeat (or cardiac cycle). The locations of different points on the ECG signal (such as the P , Q , R , S , and T waves) are determined by the parameters θ_i , a_i , and b_i in (1), where $i \in \{P, Q, R, S, T\}$. Parameters θ , a and b determine fixed angles on the unit circle, amplitudes and durations, respectively. We kindly refer the readers to Appendix A for more details about the parameters.

Solving Method of ODEs. The equations given by (1) are integrated numerically using a fourth-order Runge-Kutta method [Butcher, 1987] with a fixed time step $\Delta t = 1/f_s$, where $f_s = 1000$ is the sampling frequency. Specifically, we adopt the simplest form of the Runge-Kutta family, the Euler method [Atkinson, 1991]. The Euler method is based on the finite difference approximation [Milne-Thomson, 2000]:

$$\frac{du}{dt}(t) \approx \frac{u(t + \Delta t) - u(t)}{\Delta t}. \quad (2)$$

Given an ODE of the form $du/dt = v$, substituting it into the formula (2) yields:

$$u(t + \Delta t) = u(t) + v(t)\Delta t. \quad (3)$$

We iterate equation (3) for L time steps, where the l -th step corresponds to $t_l = l\Delta t$, and L is the number of sample points in a single signal. We then obtain:

$$u_{l+1} = u_l + v_l \Delta t. \quad (4)$$

Substitute (1) into (4) yields:

$$\begin{aligned} t_l &= l\Delta t, \\ x_{l+1} &= x_l + f_x(x_l, y_l; \eta)\Delta t, \\ y_{l+1} &= y_l + f_y(x_l, y_l; \eta)\Delta t, \\ z_{l+1} &= z_l + f_z(x_l, y_l, z_l, t_l; \eta)\Delta t. \end{aligned}$$

3.3 Denoising Diffusion Probabilistic Model

Denoising Diffusion Probabilistic Models (DDPM) [Sohl-Dickstein *et al.*, 2015; Ho *et al.*, 2020] are latent variable models that include a forward process or diffusion process where data is gradually diffused by adding Gaussian noise until it reaches a Gaussian distribution, and a reverse process where the noise is converted back into samples from the target distribution.

Diffusion Process. Diffusion process gradually adds Gaussian noise to the data $\mathbf{x}_0 \sim q(\mathbf{x}_0)$ over T iterations, which is set to a simple parameterization of a fixed Markov Chain as each step:

$$\begin{aligned} q(\mathbf{x}_{1:T}|\mathbf{x}_0) &= \prod_{t=1}^T q(\mathbf{x}_t|\mathbf{x}_{t-1}), \\ q(\mathbf{x}_t|\mathbf{x}_{t-1}) &= \mathcal{N}(\mathbf{x}_t; \sqrt{1 - \beta_t}\mathbf{x}_{t-1}, \beta_t\mathbf{I}), \end{aligned}$$

where $\mathbf{x}_1, \dots, \mathbf{x}_T$ are the latent variables with the same dimensionality as \mathbf{x}_0 , β_1, \dots, β_T is a variance schedule (either learned or fixed) which ensures that \mathbf{x}_T approximates

a standard normal distribution for sufficiently large T , and $\mathcal{N}(\mathbf{x}; \mu, \Sigma)$ is a Gaussian Probability Density Function (PDF) with parameters μ and Σ . The sampling of \mathbf{x}_t at an arbitrary timestep t has the closed-form of $q(\mathbf{x}_t|\mathbf{x}_0) = \mathcal{N}(\mathbf{x}_t; \sqrt{\bar{\alpha}_t}\mathbf{x}_0, (1 - \bar{\alpha}_t)\mathbf{I})$, where $\bar{\alpha}_t = \prod_{s=1}^t \alpha_s$ and $\alpha_s = 1 - \beta_s$. Thus \mathbf{x}_t can be expressed directly as $\mathbf{x}_t = \sqrt{\bar{\alpha}_t}\mathbf{x}_0 + (1 - \bar{\alpha}_t)\epsilon$, where $\epsilon \sim \mathcal{N}(\mathbf{0}, \mathbf{I})$.

Reverse Process. Reverse process learns to invert the above diffusion process, restoring \mathbf{x}_t to \mathbf{x}_0 . Starting from pure Gaussian noise drawn from $p(\mathbf{x}_T) = \mathcal{N}(\mathbf{x}_T; \mathbf{0}, \mathbf{I})$, the reverse process is defined by the following Markov Chain:

$$p_\theta(\mathbf{x}_{0:T}) = p(\mathbf{x}_T) \prod_{t=1}^T p_\theta(\mathbf{x}_{t-1}|\mathbf{x}_t), \mathbf{x}_T \sim \mathcal{N}(\mathbf{0}, \mathbf{I}),$$

$$p_\theta(\mathbf{x}_{t-1}|\mathbf{x}_t) = \mathcal{N}(\mathbf{x}_{t-1}; \mu_\theta(\mathbf{x}_t, t), \sigma_\theta(\mathbf{x}_t, t)\mathbf{I}).$$

In DDPM's setting, $\mu_\theta(\mathbf{x}_t, t)$ and $\sigma_\theta(\mathbf{x}_t, t)$ are defined as follows:

$$\mu_\theta(\mathbf{x}_t, t) = \frac{1}{\alpha_t} \left(\mathbf{x}_t - \frac{\beta_t}{\sqrt{1 - \alpha_t}} \epsilon_\theta(\mathbf{x}_t, t) \right),$$

$$\sigma_\theta(\mathbf{x}_t, t) = \sqrt{\tilde{\beta}_t}, \tilde{\beta}_t = \begin{cases} \frac{1 - \alpha_{t-1}}{1 - \alpha_t} \beta_t, & t > 1 \\ \beta_1, & t = 1 \end{cases},$$

where $\epsilon_\theta(\cdot, \cdot)$ is a learnable denoising function used to predict the noise vector ϵ added to \mathbf{x}_t . Our objective is to optimize the following alternative loss function:

$$Loss(\theta) = \mathbb{E}_{t, \mathbf{x}_0, \epsilon} [\|\epsilon - \epsilon_\theta(\mathbf{x}_t, t)\|^2],$$

where t is uniform between 1 and T .

3.4 Dynamic Cross-Attention Mechanism

We integrate the EPK into each block during the denoising process by utilizing the DCA mechanism, as shown in Figure 2 (a). Given that the DCA mechanism is a plug-and-play method, we specifically combine DCA with Residual Block [Kong *et al.*, 2021] due to its effective framework for waveform generation. And we name this combination RBDCA. In each RBDCA, as shown in Figure 2 (b), we use a Bidirectional Dilated Convolution (Bi-DilConv) with kernel size 3, where the dilation is doubled at each layer within each block, *i.e.*, $[1, 2, 4, \dots, 2^{n-1}]$. The value of n is related to the number of RBDCA. Specifically, the model is composed of N RBDCA, which are grouped into m parts and each part has $n = N/m$ RBDCA. Here, $N = 30$, $m = 3$ and $n = 10$.

During the Bi-DilConv process, we use an encoder τ_θ to encode signals \mathbf{x}_{ode} synthesized by the ODE system (*i.e.*, EPK). Then, we can obtain $\mathbf{y}_{ode} = \tau_\theta(\mathbf{x}_{ode})$ and an intermediate representation \mathbf{y}_{inter} after Bi-DilConv, which are then fused by our proposed DCA mechanism, as shown in Figure 2 (c). The process can be formulated as follows:

$$DCA = (\alpha(\text{Attention}_1) + (1 - \alpha)\text{Attention}_2) \cdot \mathbf{V},$$

where $\text{Attention}_i = \text{softmax}(\mathbf{Q}_i \mathbf{K}^T / \sqrt{d})$, $i = \{1, 2\}$. Here, $\mathbf{Q}_1 = \mathbf{Q}_{ode} = \mathbf{W}^{q_1} \cdot \mathbf{y}_{ode}$, $\mathbf{Q}_2 = \mathbf{Q}_{inter} = \mathbf{W}^{q_2} \cdot \mathbf{y}_{inter}$, $\mathbf{K} = \mathbf{W}^k \cdot \mathbf{y}_{ode}$, $\mathbf{V} = \mathbf{W}^v \cdot \mathbf{y}_{ode}$. And \mathbf{W}^{q_1} , \mathbf{W}^{q_2} , \mathbf{W}^k and \mathbf{W}^v are learnable projection matrices [Vaswani *et*

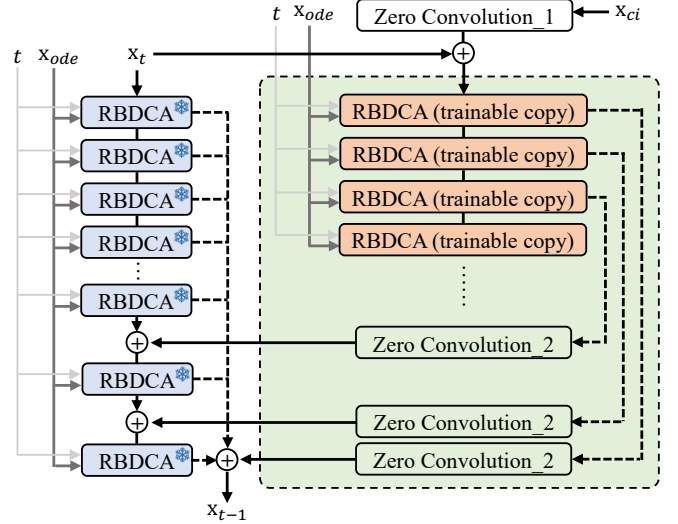


Figure 3: The architecture of CICN.

al., 2017]. $\alpha \in [0, 1)$ is the result of a fully connected layer's prediction for time-step t , used to measure the weight of EPK in the fusion process. The larger the value of α , the greater the proportion of external EPK, and vice versa. Although the design of DCA is straightforward, its innovation lies in dynamically adjusting the constraints of EPK without introducing redundant operations, which is well-suited for our task. The comparative experiments with other attention mechanisms are presented in Section 4.7.

3.5 Clinical Information ControlNet

We design Clinical Information ControlNet (CICN) to accurately simulate the individual cardiac drug reactions on ECGs. Different from the original ControlNet, CICN not only inherits the capability to ensure authenticity from the backbone diffusion model, but can also generate ECGs affected by different drugs at various time points post-dose by changing the input of clinical data.

CICN consists of three types of neural network blocks, which are $\mathbf{f}'_{rbdca}(\cdot; \theta'_{rbdca})$, $\mathbf{z}_1(\cdot; \theta_{z1})$, and $\mathbf{z}_2(\cdot; \theta_{z2})$, corresponding respectively to RBDCA (trainable copy), Zero Convolution_1, and Zero Convolution_2 in Figure 3. Following the setting of [Zhang *et al.*, 2023], $\mathbf{f}'_{rbdca}(\cdot; \theta'_{rbdca})$ is the trainable copy from the original block \mathbf{f}_{rbdca} with parameters θ_{rbdca} . $\mathbf{z}(\cdot; \cdot)$ is a 1D convolution layer with both weight and bias initialized to zeros. To build up CICN, we use two instances of zero convolutions with parameters θ_{z1} and θ_{z2} . $\mathbf{z}_1(\cdot; \theta_{z1})$ is used to process the input clinical information, while $\mathbf{z}_2(\cdot; \theta_{z2})$ is connected to the locked model. The complete CICN then computes:

$$\mathbf{y}_{ci} = \mathbf{z}_2(\mathbf{f}'_{rbdca}(\mathbf{x}_t + \mathbf{z}_1(\mathbf{x}_{ci}; \theta_{z1}); \theta'_{rbdca}); \theta_{z2}),$$

where \mathbf{x}_{ci} and \mathbf{y}_{ci} are the input and output of CICN, respectively. \mathbf{x}_{ci} includes demographic information and drug data, which is a kind of tabular data. During the training process of CICN, the parameters θ_{rbdca} of the original block are frozen. We only update the parameters of CICN. The total loss func-

Methods	QT_c Interval		PR Interval		$T_{peak} - T_{end}$ Interval	
	Accuracy (\uparrow)	Recall (\uparrow)	Accuracy (\uparrow)	Recall (\uparrow)	Accuracy (\uparrow)	Recall (\uparrow)
<i>Generative Adversarial Networks</i>						
WGAN	74.96%	75.00%	74.96%	73.53%	78.53%	80.36%
StyleGAN	73.59%	70.00%	75.13%	73.53%	77.34%	78.55%
ECG ODE-GAN	63.20%	55.00%	62.69%	58.82%	74.11%	72.73%
TTS-CGAN	70.53%	72.50%	70.53%	76.47%	83.48%	82.55%
CECG-GAN	73.59%	75.00%	72.91%	70.59%	78.19%	77.09%
<i>Diffusion Models</i>						
DiffECG	<u>83.48%</u>	<u>77.50%</u>	83.65%	<u>82.35%</u>	<u>85.86%</u>	<u>85.45%</u>
BioDiffusion	80.41%	72.50%	<u>85.01%</u>	79.41%	83.82%	83.64%
<i>Autoregressive Models</i>						
Auto-TTE	62.35%	60.00%	72.40%	67.65%	71.55%	73.45%
DADM (Ours)	89.95%	87.50%	90.80%	91.18%	92.16%	93.45%

Table 1: Comparison with other methods. The best performance is bold, and the second-best performance is underlined.

tion is as follows:

$$Loss(\theta'_{rbdca}, \theta_z) = \mathbb{E}_{t, \mathbf{x}_0, \mathbf{y}, \epsilon} [\|\epsilon - \epsilon_{\theta}(\mathbf{x}_t, t, \mathbf{y}_{ode}, \mathbf{y}_{ci})\|^2],$$

where $\theta_z = \{\theta_{z1}, \theta_{z2}\}$.

4 Experiments

4.1 Dataset

We utilize two publicly available ECG datasets, including the ECGRDVQ database [Johannesen *et al.*, 2014] and the ECGDMLD database [Johannesen *et al.*, 2016]. These two datasets collectively comprise 9,443 12-lead ECGs from 44 subjects, covering the evaluation of the effects of 8 types of drug regimens. The treatment regimens include: (1) Dofetilide; (2) Lidocaine + Dofetilide; (3) Mexiletine + Dofetilide; (4) Moxifloxacin + Diltiazem; (5) Placebo; (6) Quinidine; (7) Ranolazine; (8) Verapamil. We partition the data into training and testing sets with a 4 : 1 ratio, ensuring that the proportion of ECGs affected by each drug in the training and testing sets also follows a 4 : 1 ratio. More details can be found in Appendix B.

4.2 Implementation Details

We train a generative model for each lead using 8 NVIDIA RTX 4090 GPUs. The training process is divided into two steps: (1) train a backbone DDPM that is injected with EPK via DCA; (2) train the CIGN while freezing the parameters of DDPM. We set $T = 1000$ and the forward process variances to constants increasing linearly from $\beta_1 = 10^{-4}$ to $\beta_T = 0.02$. We use Adam optimizer [Diederik and Jimmy, 2015] with a batch size of 16 and a learning rate of 2×10^{-4} . We train all models for 50 epochs. During the validation phase, we generate the corresponding post-dose ECGs at specific time points by varying the clinical data input to CIGN.

4.3 Indicator Details

To validate whether the generated ECGs accurately simulate the post-dose reactions, we evaluate the consistency of the generated ECGs and the real post-dose ECGs in terms of normality on three critical indicators. The indicators include QT_c

interval, PR interval, and $T_{peak} - T_{end}$ interval. For example, if the real post-dose ECGs indicate that the QT_c interval is normal (or abnormal), and the generated ECGs also show this indicator as normal (or abnormal), it signifies that the model accurately simulates the drug reactions. Conversely, if not, the opposite is true.

The calculation rules and normal ranges of each indicator are as follows: **QT_c interval** is the corrected QT interval, representing the time from ventricular depolarization to complete repolarization, adjusted for heart rate. Here, we use the Bazett formula for correction: $QT_c = QT/\sqrt{RR}$, where RR represents the heart rate. $QT_c \leq 450\text{ms}$ in men and $QT_c \leq 470\text{ms}$ in women are considered normal [Gupta *et al.*, 2007]. **PR interval** represents the time it takes for the electrical signal to travel from the atria to the ventricles, including atrial depolarization and the delay at the atrioventricular node. $120\text{ms} \leq PR \leq 200\text{ms}$ is normal [Kwok *et al.*, 2016]. **$T_{peak} - T_{end}$ interval** represents the late phase of ventricular repolarization and reflects the dispersion of ventricular repolarization. $80\text{ms} \leq T_{peak} - T_{end} \leq 113\text{ms}$ is considered normal [Icli *et al.*, 2015]. The onset and offset points of the three indicators are determined by ten cardiologists with at least five years of experience.

4.4 Comparison with Other Generated Methods

The comparison methods include five GAN-based methods, two DM-based methods and one AM-based method, which are **WGAN** [Arjovsky *et al.*, 2017], **StyleGAN** [Karras *et al.*, 2019], **ECG ODE-GAN** [Golany *et al.*, 2021], **TTS-CGAN** [Li *et al.*, 2022], **CECG-GAN** [Yang *et al.*, 2024], **DiffECG** [Neifar *et al.*, 2023], **BioDiffusion** [Li *et al.*, 2024], and **Auto-TTE** [Chung *et al.*, 2023]. Considering that our focus is to make the generative model simulate the signals relevant to drugs as much as possible, in addition to accuracy, we also use recall as a metric. The higher the recall rate, the greater the ability of the generative model to simulate the signals caused by different drugs.

Single Indicator Evaluation. First, we compare the performance of different methods based on single indicators. The experimental results are shown in Table 1, from which we

Methods	Lid+Dof	Mex+Dof	Mox+Dil
WGAN	39.22%	49.09%	62.75%
StyleGAN	31.37%	41.82%	70.59%
ECG ODE-GAN	27.45%	32.73%	47.06%
TTS-GAN	50.98%	30.91%	60.78%
CECG-GAN	29.41%	43.64%	45.10%
DiffECG	43.14%	61.82%	80.39%
BioDiffusion	62.75%	60.00%	64.71%
Auto-TTE	39.22%	36.36%	37.25%
DADM (Ours)	76.47%	61.82%	<u>76.47%</u>

Table 2: Comparison with other methods in simulating composite drug reactions. Lid, Dof, Mex, Mox, and Dil respectively represent Lidocaine, Dofetilide, Mexiletine, Moxifloxacin, and Diltiazem.

Methods	FRD (\downarrow)	RMSE (\downarrow)
WGAN	1.3466	0.2328
StyleGAN	1.7853	0.3021
ECG ODE-GAN	2.5639	0.3764
TTS-GAN	0.7880	0.0716
CECG-GAN	0.7336	0.0728
DiffECG	0.5322	0.0412
BioDiffusion	<u>0.4832</u>	<u>0.0343</u>
Auto-TTE	2.5234	0.4162
DADM (Ours)	0.2431	0.0127

Table 3: Evaluation of the fidelity of ECGs generated by different generative models. The best performance is bold, and the second-best performance is underlined.

have several observations: (1) Our method achieves the highest accuracy and recall across all three indicators, demonstrating its superiority. For example, in terms of the QT_c interval indicator, our method improves the accuracy by 6.47% and the recall by 10% compared to the second-best method; (2) Although other DM-based methods perform worse than our approach, they still outperform GAN-based methods, indicating that DM-based methods are better suited for our generative task; (3) While the ECG ODE-GAN model also incorporates EPK through ODEs during the generation process, its performance is inferior to our method. This highlights the critical importance of the EPK integration strategy and, indirectly, underscores the superiority of DCA mechanism.

Multi-Indicator Evaluation. Furthermore, we compare the models’ ability to simulate the composite effects of drug combinations on ECG, including **Lidocaine + Dofetilide**, **Mexiletine + Dofetilide**, and **Moxifloxacin + Diltiazem**. We jointly evaluate several indicators among the three to reflect the models’ ability to simulate composite effects. For example, in the third combination, Moxifloxacin may prolong the QT interval, and Diltiazem may prolong the PR interval. Thus, the results are only considered correct if the model accurately simulates both indicators. We calculate the accuracy of different models based on this criterion. The experimental results are shown in Table 2, from which we can observe that (1) DADM achieves the best or second-best results in all

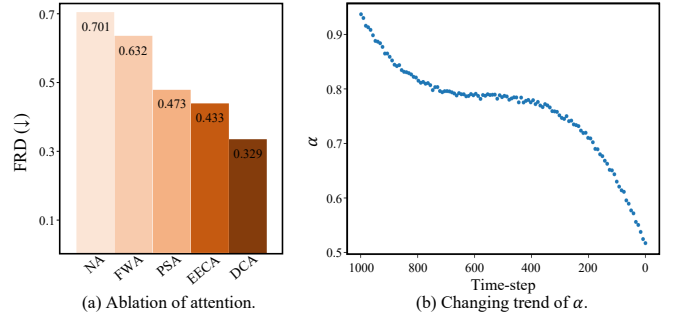


Figure 4: (a) Ablation study of attention mechanisms; (b) Changing trend of α over time-steps.

cases. Although DM-based DiffECG achieves the best performance in the second and third cases, the performance of DADM is more stable; (2) Compared to single indicator evaluation tasks, the accuracy of all methods has dropped significantly, often falling below 50%, indicating that simulating composite drug reactions remains challenging.

4.5 Evaluation of Generated ECG Fidelity

Quantitative Evaluation. The Fréchet Inception Distance (FID) [Heusel *et al.*, 2017] is a traditional metric used for assessing the fidelity of generated images. Following Hu *et al.* [2024], we introduce the Fréchet ResNet Distance (FRD) as the metric to evaluate the generated ECG fidelity. Specifically, we utilize a 1D ResNet model [Hong *et al.*, 2020] pre-trained on Challenge 2017 data [Clifford *et al.*, 2017] instead of the Inception V3 [Szegedy *et al.*, 2016] as the backbone for feature extraction from ECG data. We use the output from the network’s final fully connected layer as a feature vector to calculate the FRD on the test set. In addition, we adopt Root Mean Squared Error (RMSE) as a metric to evaluate the similarity between the generated and real ECGs post-dose. Lower FRD scores and RMSE indicate that the distribution of generated ECGs is closer to that of real ECGs. We compare the average FRD scores and RMSE of 12-lead ECGs generated by different methods, and the results are presented in Table 3. Our findings demonstrate that our method achieves the optimal FRD score of 0.2431 and an RMSE of 0.0127.

Expert Evaluation. We select 100 generated ECGs and 100 real ECGs of lead II, and then invite ten cardiologists with at least five years of experience to distinguish whether they are real or generated. The results show that $93.80\% \pm 2.66\%$ (mean \pm std) of the generated ECGs are considered to be real, demonstrating the realism of our generated ECGs.

4.6 Evaluation of Downstream Classification Task

To validate that the ECGs generated by our method improve the performance of classification models in downstream tasks, we design a binary classification experiment for drug effects (specifically Quinidine). We train four ResNet-1D models using the following datasets to classify whether the drug is administered: 1) 1,000 real ECGs, 2) 1,000 real + 100 generated ECGs, 3) 1,000 real + 200 generated ECGs, and 4) 1,000 real + 500 generated ECGs. The test set is identical for all models, consisting of 100 pre-dose and 100 post-

dose ECGs. The results are shown in Table 4, demonstrating that our generated data helps improve the performance of drug classification models. More importantly, the cost of generating data is significantly lower than that of acquiring real data. Our method provides a viable solution to the problem of data scarcity in real medical scenarios.

Dataset	Accuracy
1,000 real ECGs	92.00%
+100 generated ECGs	94.00%
+200 generated ECGs	95.50%
+500 generated ECGs	97.75%

Table 4: Evaluation of Quinidine efficacy classification accuracy with varying numbers of generated ECGs.

4.7 Ablation Study

To validate the importance of EPK and the effectiveness of DCA, we compare the FRD scores of ECGs generated using DCA with those generated using two baseline attention mechanisms and two widely-used attention mechanisms in time series analysis, including no attention (NA), fixed-weight attention (FWA), prob-sparse attention (PSA) [Zhou *et al.*, 2021], and exogenous-to-endogenous cross-attention (EECA) [Wang *et al.*, 2024]. NA means without fusing EPK, and the α of FWA is fixed at 0.5. For a fair comparison, the generative model with DCA does not have a CICN module. The experimental results are presented in Figure 4 (a), from which we have several observations: (1) Generated ECGs integrated with EPK exhibit lower FRD scores compared to those without EPK fusion, proving the effectiveness of incorporating EPK. (2) DCA outperforms other static fusion mechanisms, demonstrating that dynamically adjusting EPK’s constraints is effective and particularly well-suited for our task.

Moreover, we analyze the trend of the dynamic parameter α as it varies with the time-step t to validate the effectiveness of DCA, as shown in Figure 4 (b). In the initial stage of the denoising period, the value of α is relatively high, indicating that EPK plays a crucial role in generating the basic ECG waveform. In the later stage, α gradually decreases, suggesting that the constraints imposed by EPK diminish, allowing the generated ECGs to exhibit more diverse details.

4.8 Visualization

Visualization of ECGs With and Without EPK. To provide a more intuitive comparison of the generated ECGs with and without the introduction of EPK, we visualize the results, as shown in Figure 5. Note that in this experiment, we use the DCA mechanism to introduce EPK. Figure 5 shows that the model incorporating EPK not only captures the fundamental characteristics of heartbeats but also significantly reduces noise, thus enhancing the realism of the ECGs. In contrast, the model without EPK fails to synthesize clear waveforms, resulting in noisy signals. More visualization results can be found in Appendix C.

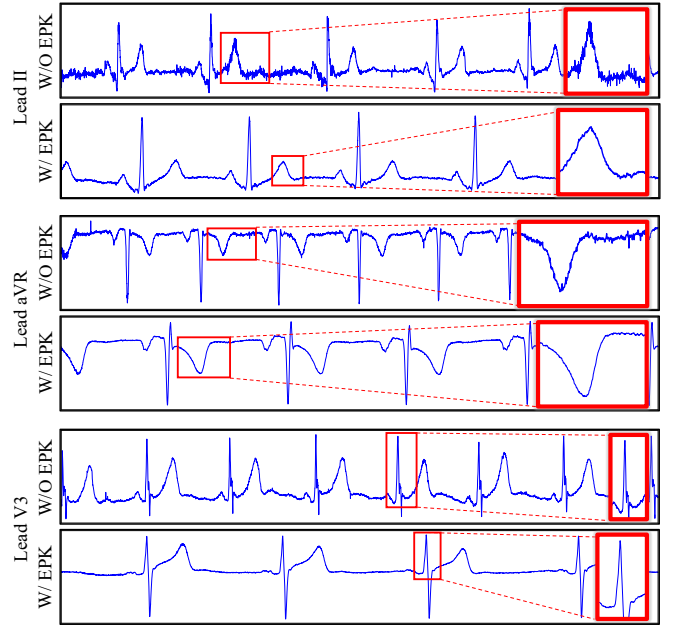


Figure 5: Visualization of generated ECGs with and without EPK. For clarity in comparison, we use the electrocardiograms of three leads: II, aVR, and V3.

Visualization of Drug Reactions. To more intuitively verify that DADM can accurately simulate the drug effects, we visualize ECGs showing the prolongation of the *PR* interval caused by Verapamil’s effect on extending atrioventricular conduction time. Specifically, we visualize the ECGs of a subject one hour after administering Verapamil. The visualization results are presented in Figure 6. It is observed that after taking Verapamil, the subject’s *PR* interval increases from 167ms pre-dose to 293ms post-dose. In the ECGs generated by our method, the *PR* interval is 270ms. Both values fall within the abnormal range, demonstrating that our method can effectively simulate the reaction of drugs on ECGs. More visualization results can be found in Appendix C.

5 Conclusions

In this paper, we design a novel framework named DADM to simulate cardiac drug reactions on ECGs for virtual clinical trials. To generate realistic ECGs, we first construct an ODE system to model EPK. Then, we propose a DCA mechanism that adaptively adjusts the constraints imposed by the EPK on ECG generation according to the time steps. To accurately simulate cardiac drug reactions, we propose a ControlNet extension called CICN to control the effects of different drugs on the ECGs according to the input clinical information. We conduct experiments across two public datasets covering 8 types of drug regimens, the results of which demonstrate superior performance of DADM over the other eight SOTA generative models in ensuring fidelity and simulating drug reactions. Furthermore, the ECGs generated by DADM can also enhance model performance in downstream drug-effect classification tasks. And the ablation and visualization results demonstrate the effectiveness of each module.

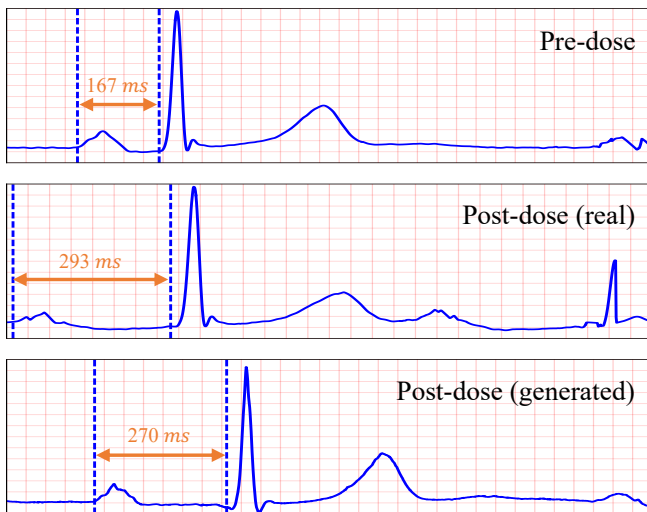


Figure 6: Visualization of Verapamil’s reactions on ECGs. Given that lead II is the most suitable for the detection of PR interval, we visualize a heartbeat from the 10-second ECGs on lead II.

6 Limitations

While our proposed DADM demonstrates potential utility in mitigating clinical trial risks by simulating drug reactions on ECGs for virtual clinical trials, several limitations still exist. First, model performance evaluation remains constrained to three fundamental cardiac indicators, which may insufficiently capture the multidimensional nature of drug toxicity. Second, the model exhibits suboptimal performance in modeling composite drug interactions. These limitations primarily stem from the limited availability of datasets, and current architectural constraints in modeling higher-order pharmacological synergies. To address these challenges, future work will focus on incorporating more comprehensive indicators (e.g., Torsades de Pointes and ST-segment depression) and modeling composite drug interactions to better approximate real-world clinical complexity.

Acknowledgements

We extend our sincere gratitude to Dr. Zheng Xiangshang and other cardiologists for their timely assistance in ECG signal analysis, including the determination of interval onset and offset locations, and the authenticity assessment of generated ECG signals.

References

Juan Miguel Lopez Alcaraz and Nils Strodthoff. Diffusion-based conditional ecg generation with structured state space models. *Computers in biology and medicine*, 163:107115, 2023.

Martin Arjovsky, Soumith Chintala, and Léon Bottou. Wasserstein generative adversarial networks. In *International conference on machine learning*, pages 214–223. PMLR, 2017.

Kendall Atkinson. *An introduction to numerical analysis*. John Wiley & sons, 1991.

John Charles Butcher. *The numerical analysis of ordinary differential equations: Runge-Kutta and general linear methods*. Wiley-Interscience, 1987.

Hyunseung Chung, Jiho Kim, Joon-myung Kwon, Ki-Hyun Jeon, Min Sung Lee, and Edward Choi. Text-to-ecg: 12-lead electrocardiogram synthesis conditioned on clinical text reports. In *ICASSP 2023-2023 IEEE International Conference on Acoustics, Speech and Signal Processing (ICASSP)*, pages 1–5. IEEE, 2023.

Gari D Clifford, Chengyu Liu, Benjamin Moody, H Lehman Li-wei, Ikaro Silva, Qiao Li, AE Johnson, and Roger G Mark. Af classification from a short single lead ecg recording: The physionet/computing in cardiology challenge 2017. In *2017 Computing in Cardiology (CinC)*, pages 1–4. IEEE, 2017.

P Davey. A new physiological method for heart rate correction of the qt interval. *Heart*, 82(2):183–186, 1999.

D Kingma Diederik and Ba Jimmy. Adam: A method for stochastic optimization. In *International Conference on Learning Representations*, 2015.

Joseph A DiMasi, Henry G Grabowski, and Ronald W Hansen. Innovation in the pharmaceutical industry: new estimates of r&d costs. *Journal of health economics*, 47:20–33, 2016.

Helen Dowden and Jamie Munro. Trends in clinical success rates and therapeutic focus. *Nat Rev Drug Discov*, 18(7):495–496, 2019.

Christopher B Fordyce, Matthew T Roe, Tariq Ahmad, Peter Libby, Jeffrey S Borer, William R Hiatt, Michael R Bristow, Milton Packer, Scott M Wasserman, Ned Braunstein, et al. Cardiovascular drug development: is it dead or just hibernating? *Journal of the American College of Cardiology*, 65(15):1567–1582, 2015.

Tomer Golany and Kira Radinsky. Pgans: Personalized generative adversarial networks for ecg synthesis to improve patient-specific deep ecg classification. In *Proceedings of the AAAI Conference on Artificial Intelligence*, volume 33, pages 557–564, 2019.

Tomer Golany, Kira Radinsky, and Daniel Freedman. Sim-gans: Simulator-based generative adversarial networks for ecg synthesis to improve deep ecg classification. In *International Conference on Machine Learning*, pages 3597–3606. PMLR, 2020.

Tomer Golany, Daniel Freedman, and Kira Radinsky. ECG ODE-GAN: Learning ordinary differential equations of ecg dynamics via generative adversarial learning. In *Proceedings of the AAAI Conference on Artificial Intelligence*, volume 35, pages 134–141, 2021.

Akshay Gupta, Andrew T Lawrence, Kousik Krishnan, Clifford J Kavinsky, and Richard G Trohman. Current concepts in the mechanisms and management of drug-induced qt prolongation and torsade de pointes. *American heart journal*, 153(6):891–899, 2007.

Martin Heusel, Hubert Ramsauer, Thomas Unterthiner, Bernhard Nessler, and Sepp Hochreiter. Gans trained by a two

- time-scale update rule converge to a local nash equilibrium. *Advances in neural information processing systems*, 30, 2017.
- Jonathan Ho, Ajay Jain, and Pieter Abbeel. Denoising diffusion probabilistic models. *Advances in neural information processing systems*, 33:6840–6851, 2020.
- Shenda Hong, Yanbo Xu, Alind Khare, Satria Priambada, Kevin Maher, Alaa Aljiffry, Jimeng Sun, and Alexey Tumanov. Holmes: health online model ensemble serving for deep learning models in intensive care units. In *Proceedings of the 26th ACM SIGKDD International Conference on Knowledge Discovery & Data Mining*, pages 1614–1624, 2020.
- Yaojun Hu, Jintai Chen, Lianting Hu, Dantong Li, Jiahuan Yan, Haochao Ying, Huiying Liang, and Jian Wu. Personalized heart disease detection via ecg digital twin generation. *arXiv preprint arXiv:2404.11171*, 2024.
- Abdullah Icli, Mehmet Kayrak, Hakan Akilli, Alpay Aribas, Mukrem Coskun, Sumeyye Fatma Ozer, and Kurtulus Ozdemir. Prognostic value of tpeak-tend interval in patients with acute pulmonary embolism. *BMC cardiovascular disorders*, 15:1–8, 2015.
- Lars Johannesen, Jose Vicente, Jay W Mason, Carlos Sanabria, Kristin Waite-Labott, Mira Hong, Ping Guo, John Lin, Jens Stampe Sørensen, Lorian Galeotti, et al. Differentiating drug-induced multichannel block on the electrocardiogram: randomized study of dofetilide, quinidine, ranolazine, and verapamil. *Clinical Pharmacology & Therapeutics*, 96(5):549–558, 2014.
- Lars Johannesen, Jose Vicente, Jay W Mason, Cassandra Erato, Carlos Sanabria, Kristin Waite-Labott, Mira Hong, John Lin, Ping Guo, Abdul Mutlib, et al. Late sodium current block for drug-induced long qt syndrome: results from a prospective clinical trial. *Clinical Pharmacology & Therapeutics*, 99(2):214–223, 2016.
- Daniel T Kaplan. Simultaneous qrs detection and feature extraction using simple matched filter basis functions. In *[1990] Proceedings Computers in Cardiology*, pages 503–506. IEEE, 1990.
- Tero Karras, Samuli Laine, and Timo Aila. A style-based generator architecture for generative adversarial networks. In *2019 IEEE/CVF Conference on Computer Vision and Pattern Recognition (CVPR)*, pages 4396–4405, 2019.
- Zhifeng Kong, Wei Ping, Jiaji Huang, Kexin Zhao, and Bryan Catanzaro. Diffwave: A versatile diffusion model for audio synthesis. In *International Conference on Learning Representations*, 2021.
- Chun Shing Kwok, Muhammad Rashid, Rhys Beynon, Diane Barker, Ashish Patwala, Adrian Morley-Davies, Duwarakan Satchithananda, James Nolan, Phyo K Myint, Iain Buchan, et al. Prolonged pr interval, first-degree heart block and adverse cardiovascular outcomes: a systematic review and meta-analysis. *Heart*, 102(9):672–680, 2016.
- Xiaomin Li, Anne Hee Hiong Ngu, and Vangelis Metsis. Tts-cgan: A transformer time-series conditional gan for biosignal data augmentation. *arXiv preprint arXiv:2206.13676*, 2022.
- Xiaomin Li, Mykhailo Sakevych, Gentry Atkinson, and Vangelis Metsis. Biodiffusion: A versatile diffusion model for biomedical signal synthesis. *Bioengineering*, 11(4):299, 2024.
- Marek Malik and A John Camm. Heart rate variability. *Clinical cardiology*, 13(8):570–576, 1990.
- Patrick E McSharry, Gari D Clifford, Lionel Tarassenko, and Leonard A Smith. A dynamical model for generating synthetic electrocardiogram signals. *IEEE transactions on biomedical engineering*, 50(3):289–294, 2003.
- Louis Melville Milne-Thomson. *The calculus of finite differences*. American Mathematical Soc., 2000.
- Nour Neifar, Achraf Ben-Hamadou, Afef Mdhaftar, and Mohamed Jmaiel. Diffecg: A versatile probabilistic diffusion model for ecg signals synthesis. *arXiv preprint arXiv:2306.01875*, 2023.
- Lorenzo Simone and Davide Bacciu. Ecgan: Self-supervised generative adversarial network for electrocardiography. In *International Conference on Artificial Intelligence in Medicine*, pages 276–280. Springer, 2023.
- Jascha Sohl-Dickstein, Eric Weiss, Niru Maheswaranathan, and Surya Ganguli. Deep unsupervised learning using nonequilibrium thermodynamics. In *International conference on machine learning*, pages 2256–2265. PMLR, 2015.
- Leif Sörnmo and Pablo Laguna. *Bioelectrical signal processing in cardiac and neurological applications*. Academic press, 2005.
- Christian Szegedy, Vincent Vanhoucke, Sergey Ioffe, Jon Shlens, and Zbigniew Wojna. Rethinking the inception architecture for computer vision. In *Proceedings of the IEEE conference on computer vision and pattern recognition*, pages 2818–2826, 2016.
- Ashish Vaswani, Noam Shazeer, Niki Parmar, Jakob Uszkoreit, Llion Jones, Aidan N Gomez, Łukasz Kaiser, and Illia Polosukhin. Attention is all you need. *Advances in neural information processing systems*, 30, 2017.
- Yuxuan Wang, Haixu Wu, Jiaxiang Dong, Guo Qin, Hao-ran Zhang, Yong Liu, Yunzhong Qiu, Jianmin Wang, and Mingsheng Long. Timexer: Empowering transformers for time series forecasting with exogenous variables. In *The Thirty-eighth Annual Conference on Neural Information Processing Systems*, 2024.
- Yang Yang, Tianyu Lan, Yang Wang, Fengtian Li, Liyan Liu, Xupeng Huang, Fei Gao, Shuhua Jiang, Zhijun Zhang, and Xing Chen. Data imbalance in cardiac health diagnostics using cecg-gan. *Scientific Reports*, 14(1):14767, 2024.
- Md Haider Zama and Friedhelm Schwenker. Ecg synthesis via diffusion-based state space augmented transformer. *Sensors*, 23(19):8328, 2023.
- Lvmin Zhang, Anyi Rao, and Maneesh Agrawala. Adding conditional control to text-to-image diffusion models. In

Proceedings of the IEEE/CVF International Conference on Computer Vision, pages 3836–3847, 2023.

Haoyi Zhou, Shanghang Zhang, Jieqi Peng, Shuai Zhang, Jianxin Li, Hui Xiong, and Wancai Zhang. Informer: Beyond efficient transformer for long sequence time-series forecasting. In *Proceedings of the AAAI conference on artificial intelligence*, volume 35, pages 11106–11115, 2021.

Technical Appendix

A Details of ODE Parameters

The ODE system is defined by 3 parameter groups, including θ_i : Phase positions governing wave event localization; a_i : Amplitude parameters controlling the wave morphology; b_i : Temporal scaling factors regulating the wave duration, where $i \in \{P, Q, R, S, T\}$. To concretely demonstrate this parametric control, Figure 7 visualizes a prototypical normal heartbeat with clinically validated reference values: $(\theta_P, \theta_Q, \theta_R, \theta_S, \theta_T) = (-\frac{1}{3}\pi, -\frac{1}{12}\pi, 0, \frac{1}{12}\pi, \frac{1}{2}\pi)$, $(a_P, a_Q, a_R, a_S, a_T) = (1.2, -5.0, 30.0, -7.5, 0.75)$, and $(b_P, b_Q, b_R, b_S, b_T) = (0.25, 0.1, 0.1, 0.1, 0.4)$. We assign values to these parameters following McSharry *et al.* [2003].

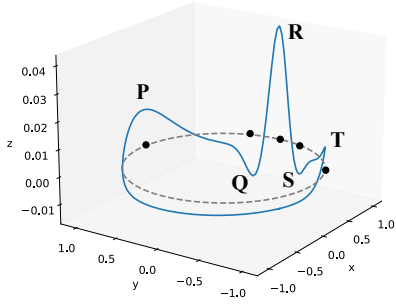


Figure 7: Visualization of the heartbeat in the 3-D space. The dashed line reflects the limit cycle of unit radius while the black points show the positions of the P , Q , R , S , and T wave events.

B Details of Datasets

ECG Recording Settings. The ECGs from the two databases are recorded at 1000Hz with an amplitude resolution of $2.5\mu\text{V}$. For ECGRDVQ database, triplicate 10-second ECGs are extracted at 16 predefined time points: 1 point pre-dose (-0.5h) and 15 points post-dose ($0.5, 1, 1.5, 2, 2.5, 3, 3.5, 4, 5, 6, 7, 8, 12, 14$, and 24h), during which the subjects were resting in a supine position for 10 minutes. For ECGDMLD database, triplicate 10-second ECGs are extracted at 14 predefined time points: 1 point pre-dose (-0.5h) and 13 points post-dose ($1.5, 2, 2.5, 3, 6.5, 7, 7.5, 8, 12, 12.5, 13, 13.5$ and 24h), during which the subjects were resting in a supine position for 10 minutes. We randomly select one ECG signal from the 3 records at each time point for experiments. We combine the pre-dose ECGs, each post-dose ECGs, and the corresponding clinical information into a single training data point. This means that for each subject, N training data points can be generated, where N represents the number of time points at which post-dose ECGs are recorded.

Clinical Information. Clinical information includes sex, age, height, weight, baseline systolic blood pressure, baseline diastolic blood pressure, race, ethnicity, sequence of treatments, visit code (PERIOD-X-Dosing refers to the X'th dosing), treatment (types of drug regimens), nominal time-point. The nominal time-point represents the time at which the post-dose ECGs are recorded.

Drug Information. The drugs in the datasets cause the following cardiac reactions: **Dofetilide** is mainly used to maintain the sinus rhythm in patients with atrial fibrillation and

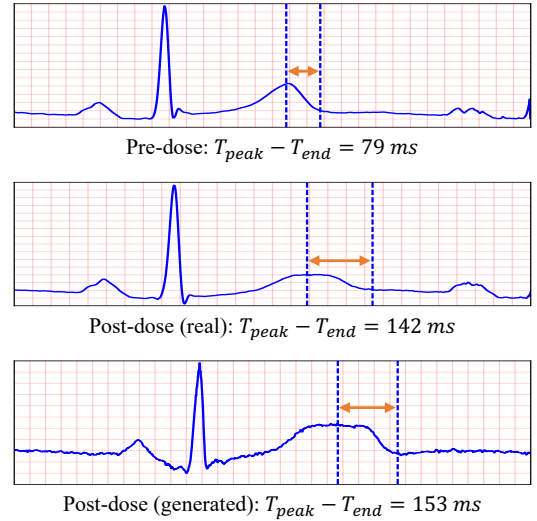


Figure 8: Visualization of Quinidine’s reactions on ECGs of lead II.

atrial flutter. It selectively blocks the delayed rectifier potassium current, prolonging the repolarization process of myocardial cells; **Lidocaine** and **Mexiletine** are mainly used for the treatment of ventricular arrhythmia. They may shorten the QT interval; **Moxifloxacin** is mainly used for the treatment of bacterial infections rather than directly targeting heart diseases. It may cause a prolongation of the QT interval; **Diltiazem** is mainly used for the treatment of arrhythmia, angina pectoris, and hypertension. It prolongs the PR interval; **Placebo** is a substance or treatment that looks like real medicine but contains no active medical ingredients. Despite having no therapeutic properties, Placebos can sometimes produce real physical or psychological benefits, known as the Placebo Effect. **Quinidine** is mainly used for the treatment of arrhythmia. It prolongs the QT interval and the width of the QRS complex; **Ranolazine** is mainly used for the treatment of chronic angina pectoris. It has a certain impact on the repolarization process of myocardial cells, which may lead to a moderate prolongation of the QT interval; **Verapamil** is mainly used for the treatment of arrhythmia, angina pectoris, and hypertension. It inhibits the influx of calcium ions, slowing down the conduction speed of the sinoatrial node and atrioventricular node, and prolonging the time it takes for the atrial impulse to be conducted to the ventricle.

C Additional Visualization Results

Figure 8 presents additional visual experimental results of drug reactions, from which we can observe that after taking Quinidine, the subject’s $T_{peak} - T_{end}$ interval increases from 79ms pre-dose to 142ms post-dose. In our generated ECGs, the $T_{peak} - T_{end}$ interval is 153ms . Both values fall within the abnormal range, demonstrating that our method can effectively simulate the reaction of drugs on ECGs. Figure 9 presents additional visual experimental results with and without EPK and drug reactions, from which we can observe that the introduction of EPK makes the generation of the ECG signal more realistic in detail. In the absence of EPK, the generated ECG signal contains a lot of noise.

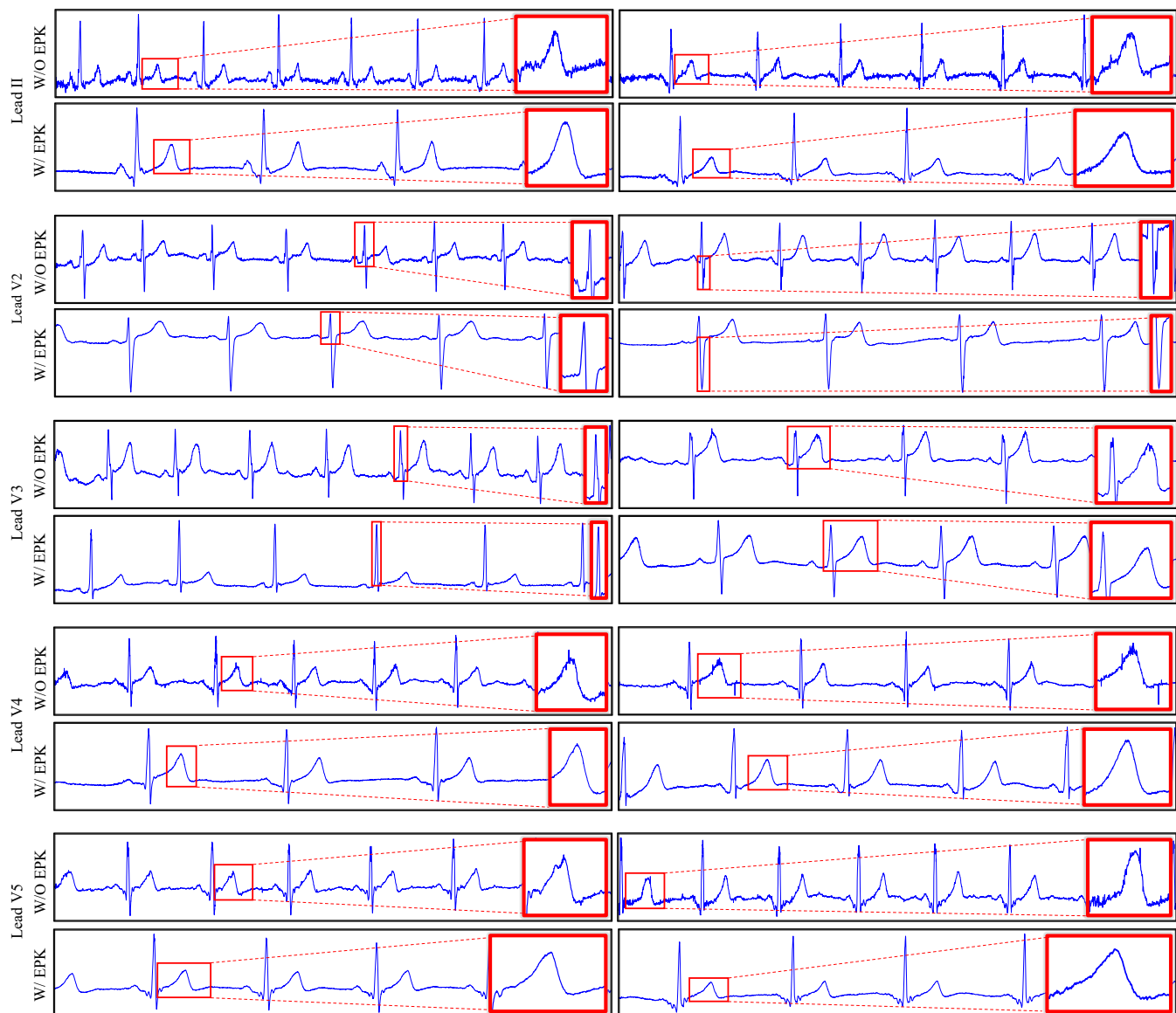


Figure 9: Additional visualization results of generated ECGs with and without EPK.